

# Balance Stabilization With Angular Momentum Damping Derived From the Reaction Null-Space

Ryotaro Hinata and Dragomir N. Nenchev

**Abstract**—A balance stabilizer is proposed that has the capability of absorbing high-energy collisions without reactive stepping. The stabilizer is based on the spatial dynamics formulation and has the unique feature that the trunk rotation can be specified in an independent way from the desired rate of change of the system (centroidal) angular momentum. The formulation is based on the momentum equilibrium principle for floating-base robots and the relativity of angular momentum revealed in the companion paper [1]. The stabilizer injects angular momentum damping via the so-called relative angular acceleration (RAA) derived from the reaction null-space (RNS) of the system. The damping is used to increase the robustness of the balance stabilizer at critical states such as foot roll. It is shown how to embed the RAA stabilizer into a joint-torque controller whereby the motion and force optimization tasks are solved in a single step, yielding a formulation that does not rely upon a general solver. The performance of the controller is examined via simulations whereby external impact-type disturbances are applied to the robot. One part of the impact energy is accommodated via the trunk rotations by lowering the respective PD feedback gains immediately after impact onset. It is then dissipated with higher gains, while recovering the stability of the posture. Another part of the impact energy yields foot roll; this part is dissipated with the angular momentum damping realized through an appropriate arm motion. When in a single stance, the angular momentum damping control yields a movement in the swing leg in addition to that in the arms. The motion in the leg injects additional angular momentum damping, such that a high-energy impact can be accommodated that would otherwise require a reactive stepping.

## I. INTRODUCTION

The simple inverted pendulum plus *reaction wheel* model was used in the design of a biped locomotion controller in [2]. It became apparent that the centroidal angular momentum and its rate of change play an important role in the balance control of humanoid robots [3]. Since then, a number of balance controllers have been designed utilizing the centroidal angular momentum based concepts, e.g. the *centroidal moment pivot* (CMP) [4], the *capture point* [5] and the *virtual repellent point* (VRP) [6]. Centroidal angular momentum control has become an indispensable part of balance controllers, especially in gait control while negotiating irregular terrain [7] or while stepping over partial footholds [8]. In the latter case, it was observed that an unstable contact could be stabilized with a lunging maneuver generated as the outcome of a spatial momentum optimization task.

In fact, the important role of the upper body movements in balance control has been pointed out some time ago

by a number of researchers. In [9], the trunk motion was employed to stabilize the dynamic gait of a humanoid robot. In [10], a “windmilling” movement in the arms was generated as the outcome of an iterative, quadratic-programming (QP) optimization approach. Such type of response was also produced in the field of animation [11]. The centroidal momentum balance controller in [12] generated an “unintentional” arm motion.

The balance controllers developed so far are based almost exclusively on the simple reaction-wheel on inverted pendulum model, and hence, on the centroidal angular momentum and its rate of change. Note, however, that although useful the model cannot completely reveal the mechanism behind the above mentioned complex upper-body motion behaviors, including the movements in the upper limbs. It should also be noted that research in the field of underactuated robots on a floating-base, such as free-floating space robots, manipulators mounted on a flexible base and macro-mini manipulators (i.e. a small-size manipulator mounted at the tip of a large-size one), has shown that the centroidal angular momentum can be expressed as the sum of two components: a *composite rigid-body* (CRB) component that is determined by a system state with locked joints, and the *coupling angular momentum* component [13]. The latter depends on the joint rates; the joint rates are mapped via the coupling inertia matrix, i.e. via a coordinate form representation of the so-called *mechanical connection*. The substantial role of this map in the modeling and control of underactuated systems in general is well known [14], [15]; in the field of humanoid robotics, though, little attention has been paid so far.

Insight into the role of the coupling angular momentum in velocity-based whole-body balance control of a humanoid robot is given in the companion paper [1]. It is pointed out that the coupling angular momentum is always in dynamic equilibrium with the *relative angular momentum*. This relation represents the *momentum equilibrium principle* in balance control. Based on this principle, the relative angular momentum/velocity (RAM/V) controller was designed. One unique feature of this controller is that trunk rotation can be specified as a motion subtask that is independent from the centroidal momentum control subtask. Another unique feature of the RAM/V controller is that foot rotation can be stabilized by making use of a reactionless motion generated from within the reaction null space (RNS) that is the null space of the coupling inertia matrix [13].

The aim of this work is to present a second-order, acceleration-based formulation of the RAM/V controller, referred to as the *relative angular acceleration* (RAA) stabilizer.

The authors are with the Graduate School of Engineering, Tokyo City University, Tamazutsumi 1-28-1, Setagaya-ku, Tokyo 158-8557, Japan. Corresponding author: D. Nenchev (Y. Kanamiya) nenchev@ieee.org

With the RAA stabilizer, angular momentum damping can be injected into the system to increase the robustness of torque-based whole-body balance control. We focus on the handling of critical states such as a rolling foot. The robot may arrive at a critical state either by an infeasible input (self-destabilization) or by an external impact. It will be shown how to embed the RAA stabilizer into a torque controller. The torque controller can ensure an appropriate body-wrench (gravity plus spatial momentum) distribution at the contacts, via the divergent-component-of-motion (DCM) generalized inverse [16], taking into account the friction cone constraints and the constraints that keep the net center of pressure (CoP) within the base-of-support (BoS). The performance of the RAA controller will be examined through simulations with impact scenarios in two critical situations. First, the capability of the controller to accommodate an impact in a double stance, with a posture such that the net CoP is located within the vicinity of the BoS boundary will be demonstrated. Second, the capability of accommodating a high-energy impact when in a single stance will be demonstrated. The magnitude of the impact is such that if the existing (capturability) theories [17] were used, a reactive step would be required to accommodate it.

## II. BACKGROUND AND NOTATION

The generalized coordinate vector of a floating-base robot is denoted by  $\mathbf{q} = (\mathcal{X}_B, \boldsymbol{\theta})$ .  $\boldsymbol{\theta} \in \mathbb{R}^n$  is the joint variable vector,  $\mathcal{X}_B \in SE(3)$  is the position and orientation of the (non-actuated) base (or root) link. The generalized velocity is defined as a *quasivelocity*, i.e. as a velocity expressed relative to a configuration-dependent frame [18]. Note that the quasivelocity is not necessarily the time derivative of the generalized coordinates. Let  $\mathcal{V}_B = [\mathbf{v}_B^T \ \boldsymbol{\omega}_B^T]^T$  denote the twist of the base link;  $\mathbf{v}_B, \boldsymbol{\omega}_B \in \mathbb{R}^3$  are the velocity of a fixed point on the base-link (e.g. the origin of the coordinate frame) and the angular velocity, respectively. These and all other quantities are expressed in the inertial frame. Furthermore, let  $\mathcal{V}_M = [\mathbf{v}_C^T \ \boldsymbol{\omega}_B^T]^T$  denote a twist of a ‘‘mixed’’ character, where  $\mathbf{v}_C$  is the velocity of the center of mass (CoM) of the robot. Two quasivelocity vectors can then be specified as  $\dot{\mathbf{q}}_B = [\mathcal{V}_B^T \ \dot{\boldsymbol{\theta}}^T]^T$  and  $\dot{\mathbf{q}}_M = [\mathcal{V}_M^T \ \dot{\boldsymbol{\theta}}^T]^T$ . Note that there is some abuse in the notation: the over-dot in  $\dot{\mathbf{q}}_{(\circ)}$  does not necessarily imply the integrability of this quantity.

### A. Equation of motion

The equation of motion, of the unconstrained humanoid robot can be written as follows [19]:

$$\begin{bmatrix} \mathbb{M}_C & \mathbf{H}_{CM} \\ \mathbf{H}_{CM}^T & \mathbf{M}_\theta \end{bmatrix} \begin{bmatrix} \dot{\mathcal{V}}_M \\ \dot{\boldsymbol{\theta}} \end{bmatrix} + \begin{bmatrix} \mathcal{C} \\ \mathbf{c}_\theta \end{bmatrix} + \begin{bmatrix} \mathcal{G} \\ \mathbf{0} \end{bmatrix} = \begin{bmatrix} \mathbf{0} \\ \boldsymbol{\tau} \end{bmatrix} + \begin{bmatrix} \mathbb{C}_c \\ \mathcal{J}_c^T \end{bmatrix} \bar{\mathcal{F}}^c, \quad (1)$$

where

$\mathbb{M}_C$	$\in \mathbb{R}^{6 \times 6}$	: CRB inertia tensor w.r.t. the CoM,
$\mathbf{M}_\theta$	$\in \mathbb{R}^{n \times n}$	: link inertia matrix,
$\mathbf{H}_{CM}$	$\in \mathbb{R}^{6 \times n}$	: coupling inertia matrix,
$\mathcal{C}$	$\in \mathbb{R}^6$	: CRB and coupling nonlinear force,
$\mathbf{c}_\theta$	$\in \mathbb{R}^n$	: link nonlinear force,
$\mathcal{G}$	$\in \mathbb{R}^6$	: CRB gravity force vector,
$\boldsymbol{\tau}$	$\in \mathbb{R}^n$	: joint torque vector,
$\mathbb{C}_c$	$\in \mathbb{R}^{6 \times c}$	: contact map,
$\mathcal{J}_c$	$\in \mathbb{R}^{c \times n}$	: constraint Jacobian,
$\bar{\mathcal{F}}^c$	$\in \mathbb{R}^c$	: contact (reaction) wrench,
$c$	$\in \mathbb{R}^1$	: number of the contact constraints.

The upper row of the above equation represents the spatial dynamics of the system. It is written in expanded form as:

$$\begin{bmatrix} ME & \mathbf{0} & \mathbf{0} \\ \mathbf{0} & \mathbf{I}_C & \mathbf{H}_C \end{bmatrix} \begin{bmatrix} \dot{\mathbf{v}}_C \\ \dot{\boldsymbol{\omega}}_B \\ \dot{\boldsymbol{\theta}} \end{bmatrix} + \begin{bmatrix} \mathbf{0} \\ \mathbf{c}_m \end{bmatrix} + \begin{bmatrix} \mathbf{g} \\ \mathbf{0} \end{bmatrix} = \mathbb{C}_c \bar{\mathcal{F}}^c. \quad (2)$$

$M$  is the total mass,  $E$  is the identity matrix,  $\mathbf{g}$  is the (negative) gravity force,  $\mathbf{I}_C(\mathbf{q})$  denotes the centroidal inertia matrix of the CRB,  $\mathbf{H}_C(\mathbf{q}) \in \mathbb{R}^{3 \times n}$  is the coupling inertia for the rotational motion,  $\mathbf{c}_m = \dot{\mathbf{I}}_C \boldsymbol{\omega}_B + \dot{\mathbf{H}}_C \boldsymbol{\theta}$  is a nonlinear velocity-dependent centroidal moment. Note that since the mixed quasivelocity is used in the notation, the CoM dynamics in the upper row are completely decoupled from the joint motion. This yields a significant advantage in balance controller design, as noted in [20] and also in [21].

The first-order instantaneous motion of the robot is constrained by the contacts as follows:

$$\mathbb{C}_c^T(\mathbf{q}) \mathcal{V}_M + \mathcal{J}_c(\mathbf{q}) \dot{\boldsymbol{\theta}} = \mathbf{0}. \quad (3)$$

### B. System angular velocity, the centroidal twist and the centroidal quasivelocity

The left-hand side in the lower part of (2) stands for the rate of change of angular momentum. Note that this quantity can be integrated w.r.t. time. The centroidal angular momentum of the robot is then obtained as

$$\mathbf{l}_C = \mathbf{I}_C \boldsymbol{\omega}_B + \mathbf{H}_C \dot{\boldsymbol{\theta}}. \quad (4)$$

This relation can be rewritten in terms of angular velocity by premultiplying it with  $\mathbf{I}_C^{-1}$ , i.e.<sup>1</sup>,

$$\boldsymbol{\omega}_C = \boldsymbol{\omega}_B + \mathbf{J}_\omega(\boldsymbol{\theta}) \dot{\boldsymbol{\theta}}, \quad (5)$$

where  $\boldsymbol{\omega}_C \equiv \mathbf{I}_C^{-1} \mathbf{l}_C$  and  $\mathbf{J}_\omega(\boldsymbol{\theta}) \equiv \mathbf{I}_C(\mathbf{q})^{-1} \mathbf{H}_C(\mathbf{q})$ . Matrix  $\mathbf{J}_\omega(\boldsymbol{\theta}) \in \mathbb{R}^{3 \times n}$  is a Jacobian-like quantity; it plays a significant role in the following derivations.

The above relation represents the instantaneous angular motion of the floating-base robot. Note that although  $\boldsymbol{\omega}_C$  has the meaning of an angular velocity, it does not associate with a specific physical body;  $\boldsymbol{\omega}_C$  will be therefore referred to as the *system angular velocity*. With this notation, the *centroidal twist* and the *centroidal quasivelocity* are defined as  $\mathcal{V}_C = [\mathbf{v}_C^T \ \boldsymbol{\omega}_C^T]^T$  and  $\dot{\mathbf{q}}_C = [\mathcal{V}_C^T \ \dot{\boldsymbol{\theta}}^T]^T$ , respectively.

<sup>1</sup>The CRB inertia tensor  $\mathbf{I}_C(\mathbf{q})$  is positive-definite (p.d.) at any configuration of the robot.

In the following derivations, we will make use of the time differential of (5), that is

$$\dot{\omega}_C = \dot{\omega}_B + \mathbf{J}_\omega \ddot{\theta} + \dot{\mathbf{J}}_\omega \dot{\theta}. \quad (6)$$

Angular acceleration  $\dot{\omega}_C$  will be referred to as the *system angular acceleration*.

### III. RELATIVE ANGULAR ACCELERATION

Noting that the spatial inertia of the CRB is p.d., the spatial dynamics in the upper row of (1) can be rewritten in terms of spatial acceleration by premultiplying it with  $\mathbb{M}_C^{-1}$ :

$$\mathbb{M}_C^{-1} \mathbf{H}_{CM} \ddot{\theta} + \mathbb{M}_C^{-1} (\mathcal{C}' + \mathcal{G}) = \dot{\mathcal{V}}_C - \dot{\mathcal{V}}_M, \quad (7)$$

where  $\mathcal{C}' \equiv \mathcal{C} - \mathbb{M}_C^{-1} \dot{\mathbb{M}}_C \mathcal{V}_C$ . The spatial acceleration  $\dot{\mathcal{V}}_C \equiv \mathbb{M}_C^{-1} \mathcal{C}_c \bar{\mathcal{F}}^c$  is referred to as the spatial acceleration of the system; it should be generated in compliance with the force-task constraints, i.e. the friction cone and the CoP-in-BoS constraints. The CRB spatial acceleration  $\dot{\mathcal{V}}_M$ , on the other hand, should be generated in agreement with the motion task constraints. The finite difference on the right-hand side of (7) exhibits the relative character of the spatial accelerations in a floating-base system; this character can be deduced from the momentum equilibrium principle revealed in [1].

With the notations introduced in Section II, relation (7) can be represented componentwise as

$$\mathbf{a}_g = \dot{\mathcal{V}}_{C_R} - \dot{\mathcal{V}}_{C_I} \quad (8)$$

and

$$\mathbf{J}_\omega \ddot{\theta} = \dot{\omega}_C - \dot{\omega}_B + \mathbf{I}_C^{-1} (\dot{\mathbf{I}}_C \omega_C - \mathbf{c}_m) \quad (9)$$

Vector  $\mathbf{a}_g$  stands for the acceleration of the gravity force. It is interesting to note that this quantity can also be interpreted as a relative CoM acceleration, i.e.

$$\Delta \dot{\mathcal{V}}_C = \dot{\mathcal{V}}_{C_R} - \dot{\mathcal{V}}_{C_I}.$$

The CoM acceleration component  $\dot{\mathcal{V}}_{C_R} \equiv \dot{\mathcal{V}}_C(\bar{\mathcal{F}}^c)$  stems from the reaction (contact) wrenches. This component is clearly distinguished from the inertial CoM acceleration component,  $\dot{\mathcal{V}}_{C_I} \equiv \dot{\mathcal{V}}_C$ . The reaction component  $\dot{\mathcal{V}}_{C_R}$  compensates the gravity CoM acceleration  $\mathbf{a}_g$  at all postures, for any inertial acceleration of the CoM. This means that *the effect of the gravity field on the spatial dynamics can be completely ignored*.

Next, focus on the angular acceleration relation (9). By comparison with (6) it becomes apparent that the nonlinear acceleration term  $\mathbf{I}_C^{-1} (\dot{\mathbf{I}}_C \omega_C - \mathbf{c}_m) = -\dot{\mathbf{J}}_\omega \dot{\theta}$ . The remaining two terms on the right-hand side of (9) are denoted as

$$\Delta \dot{\omega} = \dot{\omega}_C - \dot{\omega}_B. \quad (10)$$

The finite difference (10) will be referred to as the *relative angular acceleration* (RAA). This is a relativity relation; it leads us to the important conclusion that *the base rotation task (expressed with  $\dot{\omega}_B$ ) can be specified in an independent way from the system (centroidal) rotation task (expressed with  $\dot{\omega}_C$ )*. This is also true for the angular velocities, as shown in [1].

### IV. ACCELERATION-BASED CONTROL COMPONENTS

The above revelation about the possibility for independent assignment of two rotational-dynamics tasks via the angular accelerations means that three control components can be designed, with two control inputs for the linear and angular components of the dynamic CRB trajectories and a third one for the system (centroidal) rotation dynamics. As far as we know, none of the balance controllers reported so far in the literature offers the capability of an independent task assignment for the rotation of the trunk; in the existing controllers, the rotation of the trunk is solely determined by the outcome of the centroidal dynamics task, see e.g. [8], [22].

#### A. CRB trajectory tracking

Since our derivation is based on mixed quasivelocity s.t. the linear motion component of the CRB (i.e. the CoM motion) is completely decoupled from the CRB rotation, the CRB trajectory tracking task can be formulated as a kinematic control law that is conventionally used in fixed-base manipulator trajectory tracking control, i.e.

$$\dot{\mathcal{V}}_M^{ref} = \begin{bmatrix} \dot{\mathcal{V}}_C^{ref} \\ \dot{\omega}_B^{ref} \end{bmatrix} = \begin{bmatrix} \dot{\mathcal{V}}_C^{des} + K_{v_C} \dot{e}_{p_C} + K_{p_C} e_{p_C} \\ \dot{\omega}_B^{des} + K_{\omega_B} e_{\omega_B} + K_{o_B} e_{o_B} \end{bmatrix}. \quad (11)$$

$e_{p_C}, e_{o_B}, e_{\omega_B} \in \mathfrak{R}^3$  denote the errors for the CoM position, the base-link orientation<sup>2</sup> and the base-link angular velocity, respectively.  $K_{(\circ)} \in \mathfrak{R}^{3 \times 3}$  are p.d. feedback gains, determined much in the same way as used in the fixed-base robotics field. Note that  $(\circ)^{ref}$  and  $(\circ)^{des}$  are used to denote control input and desired quantities, respectively.

With regard to the CoM motion tracking component, in the case of a humanoid robot it is much more preferable to employ the DCM/VRP stabilization approach [6] in lieu of the above conventional-type feedforward plus PD feedback control. To this end, replace  $\dot{\mathcal{V}}_C^{ref}$  in (11) with

$$\dot{\mathcal{V}}_C^{ref} = \omega_X (\dot{\mathbf{r}}_X^{des} + K_X (\mathbf{r}_X^{des} - \mathbf{r}_X) - \mathbf{v}_C) \quad (12)$$

where  $\mathbf{r}_X \in \mathfrak{R}^3$  is the DCM,  $\omega_X$  is the natural angular frequency of the DCM dynamics and  $K_X$  is a p.d. feedback gain.

Assuming the contacts are stable and the Jacobian in the constrained-motion directions is full rank (i.e. the contact constraints are independent), the desired CRB trajectories can be tracked with asymptotic stability under the following kinematic control law:

$$\ddot{\theta} = -\mathcal{J}_c^+ (\mathcal{C}_c^T \dot{\mathcal{V}}_M^{ref} + \mathbf{h}_c) + \mathbf{N}(\mathcal{J}_c) \ddot{\theta}_u. \quad (13)$$

Here  $(\circ)^+$  denotes the pseudoinverse,  $\mathbf{N}(\circ)$  is a null-space projector,  $\ddot{\theta}_u$  is an arbitrary joint acceleration vector to be determined in what follows and  $\mathbf{h}_c = \dot{\mathcal{J}}_{cM} \dot{\theta} + \dot{\mathcal{C}}_c^T \mathcal{V}_M$  is a non-linear term. This control law was derived from the time differential of the instantaneous-motion constraint (3).

<sup>2</sup>We define the angular error in terms of the Euler axis/angle notation since the trunk rotation is limited.

### B. Balance stabilization with the RAA

There are ongoing efforts to develop motion/force trajectory generation methods s.t. the generated CRB trajectories will be contact-consistent. To the best of our knowledge, however, there is no such method yet. Thus, so-called ‘‘in-admissible inputs’’ [22] should be expected. Also, the errors in modeling and elsewhere may lead to contact violation, resulting e.g. in a foot roll and ultimately in the loss of balance. This problem can be addressed by adding a RAA control component in the control joint acceleration (13). To this end, determine the joint acceleration  $\ddot{\theta}_u$  in (13) with the help of the angular acceleration relation (9). As a result, one arrives at:

$$\ddot{\theta}^{ref} = -(\mathbf{E} - \bar{\mathbf{J}}_w^+ \mathbf{J}_w) \mathcal{J}_c^+ \mathbb{C}_c^T \dot{\mathcal{V}}_M^{ref} + \bar{\mathbf{J}}_w^+ \Delta \dot{\omega}^{ref} \quad (14)$$

$$+ \mathbf{N}(\mathcal{J}_c) \mathbf{N}(\bar{\mathbf{J}}_w) \ddot{\theta}_u^{ref} + \ddot{\theta}_{nl}.$$

Here  $\bar{\mathbf{J}}_w = \mathbf{J}_w \mathbf{N}(\mathcal{J}_c)$  is the restriction of  $\mathbf{J}_w$  by the null space of the constraint Jacobian. The joint acceleration component

$$\ddot{\theta}_{nl} = -(\mathbf{E} - \bar{\mathbf{J}}_w^+ \mathbf{J}_w) \mathcal{J}_c^+ \mathbf{h}_c - \bar{\mathbf{J}}_w^+ \dot{\mathbf{J}}_w \dot{\theta} \quad (15)$$

is a nonlinear velocity-dependent joint acceleration. There are three control inputs (or tasks): (1) the CRB trajectory tracking control task defined by  $\dot{\mathcal{V}}_M^{ref}$ , (2) the RAA control input,  $\Delta \dot{\omega}^{ref} = \dot{\omega}_C^{ref} - \dot{\omega}_B^{ref}$ , that is used for system (centroidal) angular momentum rate of change control and (3), an additional control input,  $\ddot{\theta}_u^{ref}$ , that can be used to control the trajectories of the swing foot (e.g. during the single stance phase of a gait) and/or to control the motion in the joints (e.g. to avoid reaching the joints limits or to inject joint damping).

The control law (14) will be referred to as the RAA balance stabilizer. Apparently, the three tasks are arranged in a hierarchical structure, as is usually done to ensure that task conflicts can be handled in an appropriate way [23]. We should note that, in our experiments, we barely encountered such conflicts, though, mainly because the Jacobian-like matrix  $\mathbf{J}_w$  becomes rarely rank-deficient.

### C. RAA input design for angular momentum damping

In order to understand the role of the independent control of the rate of change of the system (centroidal) angular momentum, consider the following two constraints for momentum conservation:

$$\dot{\omega}_C^{ref} = \mathbf{0} \Rightarrow \dot{\omega}_C^{ref} = -\mathbf{D}_\omega \omega_C, \quad (16)$$

$$\Delta \dot{\omega}^{ref} = \mathbf{0} \Rightarrow \Delta \dot{\omega}^{ref} = -\mathbf{D}_\omega \Delta \omega. \quad (17)$$

The upper constraint conserves the system (centroidal) angular momentum, the lower one conserves the coupling angular momentum.  $\mathbf{D}_\omega$  denotes a nonnegative damping gain. With these formulations, two types of angular momentum damping can be injected into the system. In this work, we focus on coupling angular momentum conservation as given in (17). As noted in [1], the coupling angular momentum control input  $\Delta \dot{\omega}^{ref} = \mathbf{0}$  will force the robot to behave as a CRB. This type of behavior can be used as a *neutral response* after

contacts destabilization. It does not guarantee, however, the recovery of the contact stability. To recover the stability, the energy that led to contact destabilization has to be dissipated. This is done with the negative damping term in (17).

### V. JOINT-TORQUE CONTROLLER

The three acceleration-based control components, discussed in the last section, can be embedded into a joint torque controller. In this way, it becomes possible to address the body-wrench distribution problem and thus, to satisfy the friction cone and the CoP-in-BoS constraints. The body wrench is the sum of the gravity wrench and the rate of change of the spatial momentum. The latter is obtained in a straightforward way from the RAA stabilizer output (14) and the reference CRB trajectories  $\dot{\mathcal{V}}_M^{ref}$  in (11) as:

$$\dot{\mathcal{L}}_C^{ref} = \mathcal{A}_C \dot{\mathbf{q}}_M^{ref} + \dot{\mathcal{A}}_C \dot{\mathbf{q}}_M \quad (18)$$

where  $\dot{\mathcal{L}}_C$  denotes the system spatial momentum and

$$\mathcal{A}_C = [\mathbb{M}_C \quad \mathbf{H}_{CM}] \in \mathbb{R}^{6 \times (6+n)}.$$

Note that  $\mathcal{A}_C$  is similar to the centroidal momentum matrix appearing in [12], [24].

The reference contact wrenches can be computed by solving an optimization task for the wrench distribution problem. Here, we employ a *noniterative* least-squares optimization approach:

$$(\bar{\mathcal{F}}^c)^{ref} = \mathbb{C}_c^{-W_{DCM}} (\dot{\mathcal{L}}_C^{ref} + \mathcal{G}) + \mathbf{N}(\mathbb{C}_c) \bar{\mathcal{F}}_u^c \quad (19)$$

where  $\mathbb{C}_c^{-W_{DCM}}$  denotes the *DCM generalized inverse* [16] that is a weighted generalized inverse of the contact map.  $\mathbf{W}_{DCM}$  stands for the weighting matrix. The null-space term on the r.h.s. is used to deal with the friction cone constraints [16].

The unique joint-space inverse dynamics (JSID) solution can be obtained from the lower row of (1) as:

$$\boldsymbol{\tau} = \mathbf{H}_{CM}^T \dot{\mathcal{V}}_M^{ref} + \mathbf{M}_\theta \ddot{\theta}^{ref} + \mathbf{c}_\theta - \mathcal{J}_c^T (\bar{\mathcal{F}}^c)^{ref}. \quad (20)$$

The block diagram of the joint-torque controller is shown in Fig. 1.

### VI. IMPACT ACCOMMODATION BY CONSERVING THE COUPLING ANGULAR MOMENTUM

In general, an impact can be accommodated with an appropriate rate of change in the linear or the angular component of the spatial momentum, or in the total spatial momentum. When the ground projection of the extrapolated CoM [25] (i.e. the instantaneous capture point (ICP) [17]) is located in the vicinity of the BoS boundary, even a low-energy impact could invoke a critical postural state leading to a foot roll. As clarified in [25], a swift action would then be required to restore the balance. Note that, at such a critical state, it would be impossible to accommodate the impact via CoM motion without taking a step. Another possibility is to employ the rate of change of the angular momentum, by rotating the trunk and the arms. This possibility will be explored below.

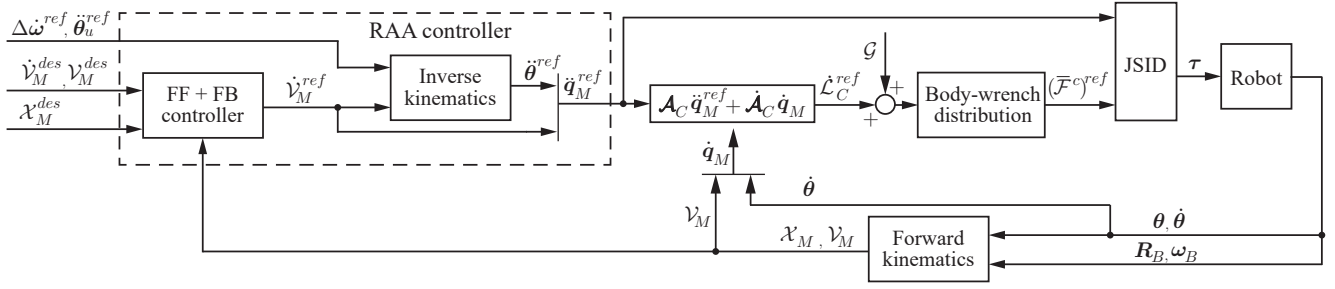


Fig. 1. Block diagram of the RAA controller embedded into a torque controller. The FF + FB controller block (FF and FB stand for “feedforward” and “feedback,” respectively) uses (11), (12). The Inverse kinematics block calculates the control joint acceleration in accordance with (14). The Body-wrench distribution block uses (19). The JSID (joint-space inverse dynamics) block is based on (20).

In the companion paper [1] it is shown that the balance control approach based on the relative angular velocity (RAV) is useful to stabilize the contacts after their destabilization via a very fast *proactive* trunk bend. The movements of the arms, though not under direct control, have been shown to play thereby an important role. The method can be adopted in a straightforward manner to generate and control the reflexive motion of a humanoid robot subjected to an impact. To ensure that impacts can be dealt with appropriately via the angular momentum damping, the second-order formulation of the method developed in this work will be employed.

As already noted, the RAA joint acceleration given in (14) comprises three independent control inputs: the (inertial) CoM acceleration,  $\dot{v}_{C_I}^{ref}$ , the angular acceleration of the base link,  $\dot{\omega}_B^{ref}$  and the system (centroidal) angular acceleration input,  $\dot{\omega}_C^{ref}$ . Since the focus is on impact accommodation via rotational motion, in the following simulations the CoM motion task will be specified as a regulation toward the initial state, with damping. Note that the initial posture will be intentionally set to be close to a critical state, i.e. the ground projection of the CoM will be in the vicinity of the toe boundary and the impact will be applied on the back. With this scenario, a foot roll can be expected. This means that the conservation of the system angular momentum, as in (16), is not an option; it would be impossible to reverse the rolling in the feet with this constraint. As shown in the companion paper [1], to reverse the foot roll and to stabilize the robot, the coupling angular momentum should be conserved in accordance with (17). Given the reference trunk rotation  $\dot{\omega}_B^{ref}$ , the system angular acceleration can be obtained from (17) as

$$\dot{\omega}_C^{ref} = \dot{\omega}_B^{ref} - D_\omega J_\omega \dot{\theta}. \quad (21)$$

## VII. EXPERIMENTS

The capability of the RNS-based postural stabilization will be demonstrated with the following two simulations<sup>3</sup>. A small-size humanoid robot HOAP-2 of mass 7 kg [27] was placed on a flat ground in a symmetric posture, the feet being aligned. The initial posture was stabilized with the asymptotic CRB trajectory tracking control laws in (11).

<sup>3</sup>The Choreonoid dynamic simulator [26] is used.

The CoM motion was regulated at the initial position. To minimize the deviation of the CoM during the impact, the respective PD feedback gains were set at relatively high values ( $K_{p_C} = 300$ ,  $K_{v_C} = 50$ ) t The damping gain in (21), that is used to enforce the RNS-based motion generation, was set at  $D_\omega = 100$ .

### A. Accommodation of an impact when in a double stance

In the first simulation, the performance of the controller at a critical state (foot roll) was examined. The robot was leaning forward s.t. the ground projection of the CoM was in the vicinity of the BoS boundary (the toe area). The critical state was invoked by an impact applied horizontally within the sagittal plane from behind. The application point was around the neck, the exact coordinates (in the base-link frame) were (0, 0, 145) [mm]. The impulse of the disturbance was of magnitude 5.5 N applied for 50 ms. Since the disturbance direction had no lateral component, it could be expected that the impulse would be accommodated with a forward bend. The angular acceleration  $\dot{\omega}_B^{ref}$  was designed as a PD feedback control law (no feedforward component) to mimic a virtual spring-damper that would ensure the compliant behavior at impact and the fast recovery after the impact. It would be sufficient to regulate the base-link angular deviation toward the initial posture during all three phases, the pre-impact, the (reflex) impact and the post-impact one.

To accommodate the impact during the reflex phase and to stabilize the posture in the post-impact phase, a gain scheduling approach was employed (see e.g. [28]). The set of the PD gains for the base rotation is given in Table I. Initially, high gains were used to ensure the desired pre-impact base orientation. After the impact onset, these gains had to be lowered as fast as possible to ensure the compliance of the trunk. In our case, the gains were lowered with a delay of 30 ms (the Impact I phase). The delay means that the robot did not expect the impact. The gains were held at low values during the remaining 20 ms of the impact (the Impact II phase). After the impact, the gains were increased to their initial values (the Post-impact I phase) to ensure swift recovery of the initial posture during the final phase (Post-impact II).

TABLE I  
GAIN SCHEDULING FOR THE VIRTUAL SPRING-DAMPER CONSTANTS OF THE BASE-LINK ROTATION (DOUBLE STANCE)

Phase	Pre-impact	Impact 1	Impact 2	Post-impact 1	Post-impact 2
Time [s]	0 ~ 1.0	1.0 ~ 1.03	1.03 ~ 1.05	1.05 ~ 1.25	1.25 ~
$K_{oB}$ (P-gain)		300	300 ~ 0.01	0.01 ~ 30	30
$K_{\omega B}$ (D-gain)		50	50 ~ 0.001	0.001 ~ 5	5

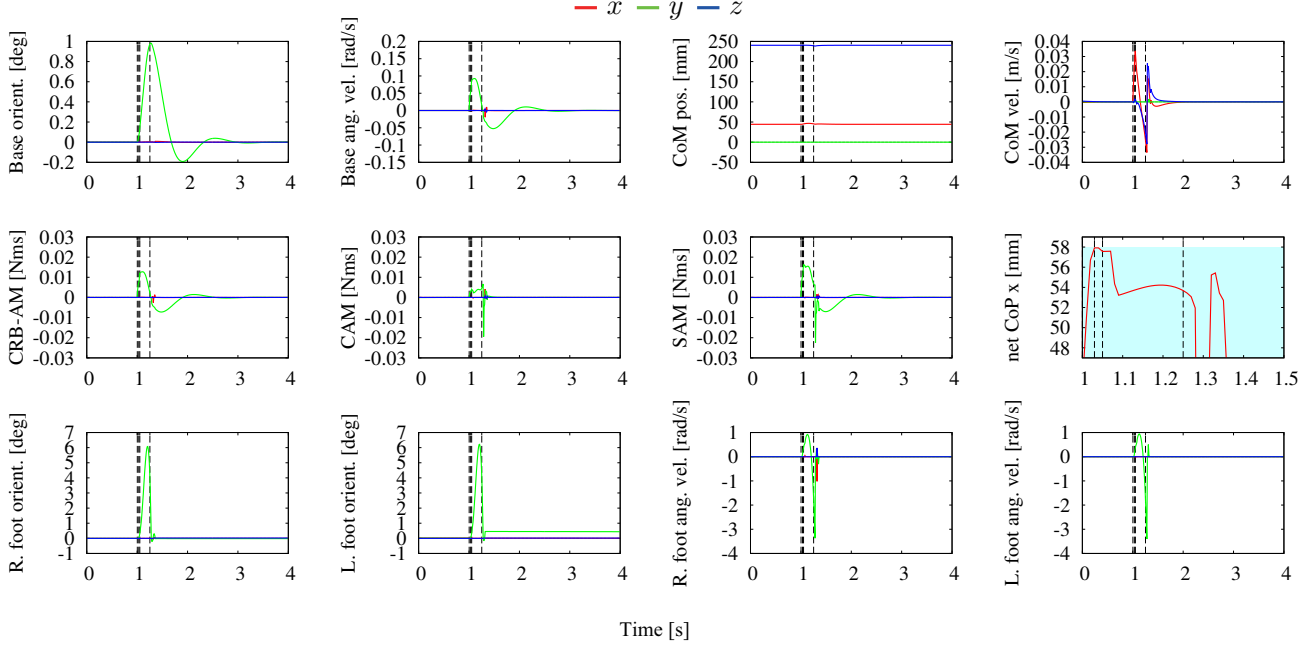


Fig. 2. Results for the reflexive impulse accommodation when in a double stance. The vertical dashed lines signify the time instants in Table I. The area colored in light-blue is the BoS.

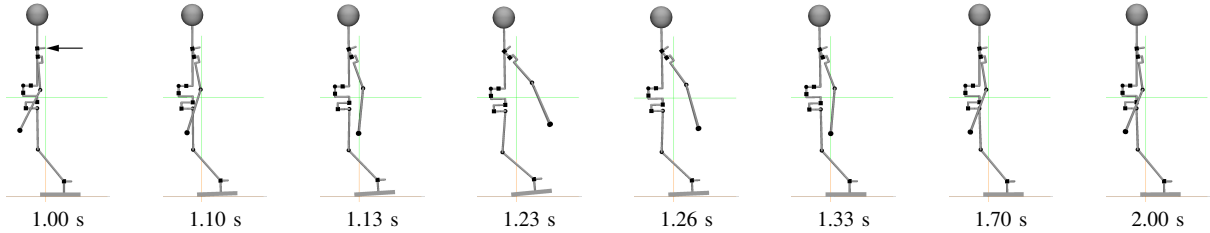


Fig. 3. Snapshots from the accommodation of an impact applied when the robot is in a double stance. The rolling feet are clearly seen in the snapshot taken at 1.23 s.

The results of the simulation are shown in an animated form in Part 1 of the accompanying video and in a graphic form in Fig. 2. Snapshots from the animation are shown in Fig. 3. The graphs are for the CoM position and velocity, the base-link orientation and angular velocity, the CRB, the coupling and the system angular momentum (abbreviated as CRB-AM, CAM and SAM, respectively), the net CoP graph in the sagittal plane and finally, for the orientations and angular velocities of the feet.

From the graphs it is seen that the impact was successfully accommodated, mainly with a base angular deviation in the pitch direction, as expected. The displacement of the CoM was insignificant. During the reflex phase, the net CoP arrived at the BoS boundary. From the foot angular velocity graphs it is seen that the feet began to roll. Nevertheless,

the RNS-based angular momentum damping injected via the motion in the arms was able to recover the plane contacts at the feet and the stability of the posture. Note that no provision was made in the controller for the contact transitions at the feet. This clearly demonstrates the robustness of the controller w.r.t. contact model discrepancies.

### B. Accommodation of a high-energy impact when in a single stance

The main idea behind accommodating a high-energy impact without stepping is to make use of the RNS based whole-body motion generation and control approach when the robot is in a single stance. The generated motion in the free leg then contributes, together with that in the torso and the upper-limb motion, to the dissipation of the energy of

the impact. In this way, a relatively large impact can be accommodated.

The initial posture was a single stance one, the left foot being lifted off the floor, the ground projection of the CoM position was well within the BoS, at  $(-25.0, -25.0)$  mm in the local frame of the right foot. A horizontal impact force of  $\mathbf{f}_{ext} = (25, 5)$  N was applied for 100 ms at the same point as in the previous simulation. The timing of the impact and the gain scheduling setting are shown in Table II.

The results from the simulation are shown in an animated form in Part 2 of the accompanying video and in graphic form in Fig. 4. Snapshots from the animation are shown in Fig. 5. From the simulation data it is apparent that the high-energy impact has been accommodated successfully. The impact induced a rotational disturbance in the support foot, but only instantaneously. The stable state was recovered swiftly with the RAA control law. The energy of the impact was dissipated in the post-impact phases, s.t. the robot came to rest without disturbing the stance foot state significantly.

From the above example it becomes apparent that with the RAA/RNS balance control approach, it is possible to accommodate relatively large impacts without taking a step.

## VIII. CONCLUSIONS

The main contribution in this work is the derivation of a second-order formulation of the RAM/V controller proposed in [1] and its application for torque-based whole-body control. With the second-order formulation it becomes possible to handle impact-type disturbances, including high-energy ones. The RAA balance controller does not rely on an iterative solver and thus, is quite efficient from a computational point of view.

We used a gain scheduling approach to vary the base-link (trunk) rotation gains. This is a heuristic approach, but there is only one simple and intuitive rule: lower the gains immediately after the impact and restore them shortly after the impact. In a future work we plan to clarify the boundary values for the gains and the timing for the scheduling in relation to the energy of the impact and the number of limbs used to generate the rate of change of the spatial momentum that is required for the damping. We also plan to explore the possibility of angular momentum damping under centroidal angular momentum conservation, both in reactive and proactive balance control tasks.

## REFERENCES

- [1] D. N. Nenchev. The momentum equilibrium principle: Foot contact stabilization with relative angular momentum/velocity. In *IEEE-RAS International Conference on Humanoid Robotics*, 2018.
- [2] J. E. Pratt. *Exploiting inherent robustness and natural dynamics in the control of bipedal walking robots*. PhD thesis, MIT, 2000.
- [3] A. Goswami and V. Kallem. Rate of change of angular momentum and balance maintenance of biped robots. In *IEEE International Conference on Robotics and Automation*, pages 3785–3790, New Orleans, LA, USA, 2004.
- [4] M. B. Popovic, A. Goswami, and H. Herr. Ground reference points in legged locomotion: Definitions, biological trajectories and control implications. *The International Journal of Robotics Research*, 24(12):1013–1032, dec 2005.

- [5] J. Pratt, J. Carff, S. Drakunov, and A. Goswami. Capture point: A step toward humanoid push recovery. In *IEEE-RAS International Conference on Humanoid Robots*, pages 200–207, Genoa, Italy, dec 2006.
- [6] J. Engelsberger, C. Ott, and A. Albu-Schaffer. Three-dimensional bipedal walking control using divergent component of motion. In *IEEE/RSJ International Conference on Intelligent Robots and Systems*, pages 2600–2607, Tokyo, Japan, nov 2013.
- [7] J. Engelsberger, C. Ott, and A. Albu-Schaffer. Three-dimensional bipedal walking control based on divergent component of motion. *IEEE Transactions on Robotics*, 31(2):355–368, apr 2015.
- [8] G. Wiedebach, S. Bertrand, T. Wu, L. Fiorio, S. McCrory, R. Griffin, F. Nori, and J. Pratt. Walking on partial footholds including line contacts with the humanoid robot Atlas. In *IEEE-RAS International Conference on Humanoid Robots*, pages 1312–1319, nov 2016.
- [9] A. Takanishi, M. Tochizawa, H. Karaki, and I. Kato. Dynamic biped walking stabilized with optimal trunk and waist motion. In *IEEE/RSJ International Workshop on Intelligent Robots and Systems*, pages 187–192, 1989.
- [10] S. Kudoh, T. Komura, and K. Ikeuchi. The dynamic postural adjustment with the quadratic programming method. In *IEEE/RSJ International Conference on Intelligent Robots and System*, pages 2563–2568, 2002.
- [11] A. Macchietto, V. Zordan, and C. R. Shelton. Momentum control for balance. *ACM Transactions on Graphics*, 28(3):80:1–80:8, 2009.
- [12] D. E. Orin, A. Goswami, and S. H. Lee. Centroidal dynamics of a humanoid robot. *Autonomous Robots*, 35(2-3):161–176, 2013.
- [13] D. N. Nenchev. Reaction Null Space of a multibody system with applications in robotics. *Mechanical Sciences*, 4:97–112, 2013.
- [14] R. M. Murray. Nonlinear control of mechanical systems: A Lagrangian perspective. *Annual Reviews in Control*, 21:31–42, 1997.
- [15] J. P. Ostrowski. Computing reduced equations for robotic systems with constraints and symmetries. *IEEE Transactions on Robotics and Automation*, 15(1):111–123, 1999.
- [16] M. Hosokawa, D. N. Nenchev, and T. Hamano. The DCM generalized inverse: Efficient body-wrench distribution in multi-contact balance control. *Advanced Robotics*, 32(14):778–797, aug 2018.
- [17] T. Koolen, T. de Boer, J. Rebula, A. Goswami, and J. Pratt. Capturability-based analysis and control of legged locomotion, Part 1: Theory and application to three simple gait models. *The International Journal of Robotics Research*, 31(9):1094–1113, jul 2012.
- [18] A. M. Bloch, J. E. Marsden, and D. V. Zenkov. Quasivelocities and symmetries in non-holonomic systems. *Dynamical Systems*, 24(2):187–222, 2009.
- [19] Y. Fujimoto, S. Obata, and A. Kawamura. Robust biped walking with active interaction control between foot and ground. In *IEEE Int. Conf. on Robotics and Automation*, pages 2030–2035, Leuven, Belgium, 1998.
- [20] S. H. Hyon, J. G. Hale, and G. Cheng. Full-body compliant human-humanoid interaction: balancing in the presence of unknown external forces. *IEEE Transactions on Robotics*, 23(5):884–898, oct 2007.
- [21] B. Henze, M. A. Roa, and C. Ott. Passivity-based whole-body balancing for torque-controlled humanoid robots in multi-contact scenarios. *The International Journal of Robotics Research*, 35(12):1522–1543, oct 2016.
- [22] S. H. Lee and A. Goswami. A momentum-based balance controller for humanoid robots on non-level and non-stationary ground. *Autonomous Robots*, 33(4):399–414, apr 2012.
- [23] D. N. Nenchev. Differential Kinematics. In Ambarish Goswami and Prahlad Vadakkepat, editors, *Humanoid Robotics: A Reference*, pages 1–47. Springer Netherlands, Dordrecht, 2018.
- [24] D. E. Orin and A. Goswami. Centroidal momentum matrix of a humanoid robot: Structure and properties. In *IEEE/RSJ International Conference on Intelligent Robots and Systems, IROS*, pages 653–659, Nice, France, 2008.
- [25] A. L. Hof, M. G. J. Gazendam, and W. E. Sinke. The condition for dynamic stability. *Journal of Biomechanics*, 38(1):1–8, jan 2005.
- [26] S. Nakaoka. Choreonoid: Extensible virtual robot environment built on an integrated GUI framework. In *IEEE/SICE International Symposium on System Integration (SII)*, pages 79–85, dec 2012.
- [27] Fujitsu. *Miniature humanoid robot HOAP-2 manual (in Japanese)*. Fujitsu Automation Co., Ltd, 1st edition, 2004.
- [28] D. J. Leith and W. E. Leithead. Survey of gain-scheduling analysis and design. *International Journal of Control*, 73(11):1001–1025, jan 2000.

TABLE II  
GAIN SCHEDULING FOR ACCOMMODATING A HIGH-ENERGY IMPACT WITHOUT STEPPING (SINGLE STANCE).

Phase	Pre-impact	Impact 1	Impact 2		Post-impact 1	Post-impact 2	
Time [s]	0 ~ 0.5	0.5 ~ 0.53	0.53 ~ 0.55	0.55 ~ 0.6	0.6 ~ 1.1	1.1 ~ 3.0	3.0 ~
$K_{oB}$ (P-gain)		300	300 ~ 0.01		0.01	0.01 ~ 300	300
$K_{\omega B}$ (D-gain)		50	50 ~ 0.001	0.001	0.001 ~ 5	5 ~ 50	50

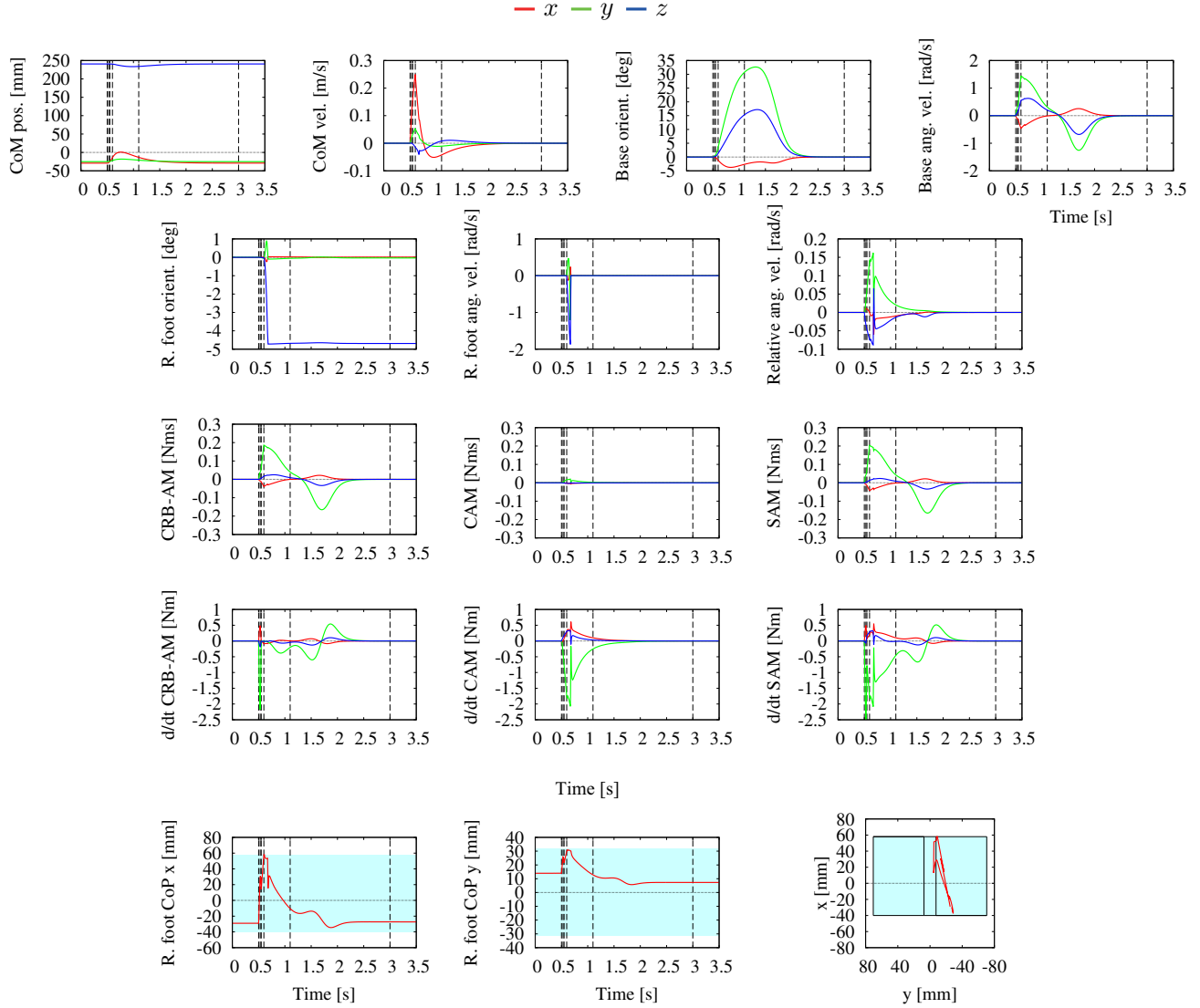


Fig. 4. Accommodation of a high-energy impact on the back without stepping. The CRB, the coupling and the system angular momentum are abbreviated as CRB-AM, CAM and SAM, respectively. The areas colored in light blue denote the BoS.

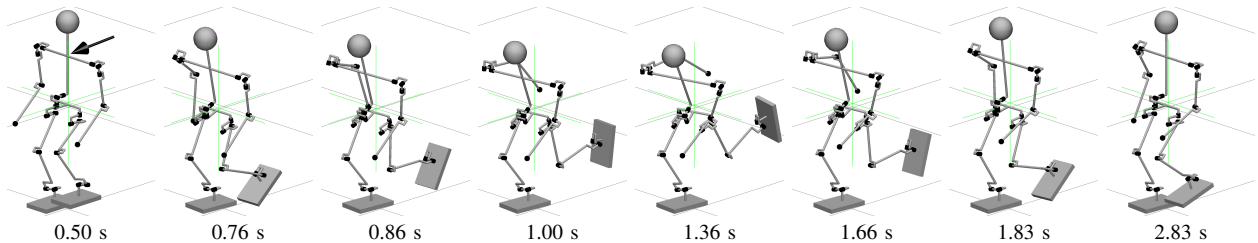


Fig. 5. Snapshots from the accommodation of a high-energy impact applied when the robot is in a single stance.